e-J. Surf. Sci. Nanotech. Vol. 7 (2009) 395-404 Conference - ICSFS-14 -

# Competing Defect Mechanisms and Hydrogen Adsorption on Li-Doped MgO Low Index Surfaces: A DFT+$U$ Study*

David O. Scanlon, Aron Walsh, Benjamin J. Morgan, and Graeme W. Watson†
*School of Chemistry, Trinity College, University of Dublin, Dublin 2, Ireland*
(Received 3 June 2008; Accepted 24 December 2008; Published 4 April 2009)

Three competing defect configurations of Li-doping of MgO on the (100), (110) and (111) low index surfaces have been investigated using GGA + $U$. The three configurations investigated on each of the surfaces were: substitution of Li for Mg with the formation of a compensating oxygen hole state ($[Li'_{Mg} - O^{\bullet}_{O}]$), substitution of Li for Mg with the addition of a Li surface interstitial ($[Li'_{Mg}Li^{\bullet}_{i}]$) and the clustering of two Li ions with the formation of a neutral $[Li'_{Mg}V^{\bullet\bullet}_{O}Li'_{Mg}]$ oxygen vacancy. The electronic structure, geometry and energetics of these defects are examined, and the effect on catalytic activity is discussed. Hydrogen abstraction from methane on the three surfaces is also investigated. Our results demonstrate that the energetics associated with hydrogen adsorption are strongly surface dependent, with the (111) oxygen terminated surface indicated as being the most promising catalytically.
[DOI: 10.1380/ejssnt.2009.395]

Keywords: Density functional calculations; Surface electronic phenomena; Catalysis; Surface defects; Magnesium oxides

## I. INTRODUCTION

Efficient transportation of natural gas from the remote locations of most natural gas reserves to the consuming facilities has long been a stumbling block in the petrochemical industry [1]. Identification of a catalyst that could transform methane into higher chain hydrocarbons (called the oxidative coupling of methane (OCM)) for ease of transport is a very important goal, and in 1985 Ito's pioneering paper on catalysis of methane coupling on Li-doped MgO [2] proved a key breakthrough. This discovery was followed by an extensive research drive into OCM which has continued even to the present day [3–7].

Li-doped MgO, when operated at high temperatures, can produce a significant fraction of $C_2$ hydrocarbons, with up to 73% selectivity at 7% Li-doping [1]. Methyl radicals are produced by methane activation at the catalyst surface [8–11], and these methyl radicals react with other methyl radicals in the gas phase [12]. The proposed reaction site for the extraction of hydrogen radicals from methane is an oxygen hole or small polaron found on the surface of the catalyst, formed when the dopant Li, having a formal charge of +1 replaces a Mg atom with a charge of +2. This unpaired electronic hole resides in the the oxygen 2$p$ band, and localizes on one of the nearest neighbour oxygens, forming a $[Li'_{Mg} - O^{\bullet}_{O}]$ defect centre. The presence of this trapped polaron on a single oxygen has been shown experimentally in high resolution energy loss spectroscopy studies (HREELS) [13], electron paramagnetic resonance studies (EPR)and electron nuclear double resonance (ENDOR) studies [14–17], by reaction with NO [17] and by electron spin resonance(ESR) studies [18, 19].

Insights into the geometry of the defect centre were also obtained by decomposition of the magnetic hyperfine interaction, although the Li–O distance calculated depended on the radial extent of the O 2$p$ orbital function applied in the analysis. Li–O distances of 2.37 – 2.59 Å were noted [14] (using a number of models), all which were considerably longer than the regular bulk Mg–O distance of 2.11 Å or the bulk Li–O distance of 2.00 Å found in $Li_2O$.

Theoretically Li-doped MgO has received considerable attention due to its interesting catalytic properties, and because the chemical bonding in MgO is highly ionic, making it very tractable by modern quantum mechanical methods [20]. Lintuluoto and Nakamura[21] used bare cluster models to study the Li-doped (100) surface and reported a single increased Li–O bond distance of 2.58 Å and analysis of their spin densities and atomic charges shows localization of the hole on the O atom with the increased Li–O bond, which is consistent with experiment [14, 15, 17].

Periodic UHF calculations [22, 23] also show an elongated Li–O bond length of $\sim$ 2.5 Å, and detailed analysis of the density of states reveals that the unpaired electron occupies an O 2$p$ orbital that is lower in energy than the onset of the valence band with an unoccupied state in the band gap. These results are again consistent with experiment [14, 15, 17].

Periodic DFT has also been used to investigate Li-doping of MgO [23, 24], but in all cases DFT fails to reproduce the localized nature of the defect state, instead producing an unpaired electron which is delocalized over the neighbouring oxygens. This failure to predict a localized defect is caused by the fact that GGA (or LDA) functionals do not contain exact exchange, and thus cannot cancel the unphysical electron self interaction [25].

This problem of localizing O 2$p$ holes in doped metal oxides has been noted before [26–28], and is also a problem in systems with localized 3$d$ ($V_2O_5$ [29], $TiO_2$ [30]) and 4$f$ ($CeO_2$ [31]) states. One method commonly used to combat this self interaction error is to use GGA + $U$, which is GGA corrected for on-site Coulomb interactions for strongly correlated systems. This has been shown to give much improved descriptions of localized systems [32–34]. In this context GGA + $U$ has been used to study Li-doping of MgO previously, and gives results in agreement with both experimental data and the previous UHF calculations [35, 36].

In the present paper we present a detailed study of Li-doped MgO using GGA + $U$, including analysis of three

*This paper was presented at the 14th International Conference on Solid Films and Surfaces (ICSFS-14), Trinity College Dublin, Ireland, 29 June - 4 July, 2008.
†Corresponding author: watsong@tcd.ie

  

possible competing defect conformations on the low index surfaces of MgO; substitution of Li for Mg with the formation of a compensating oxygen hole state $[Li'_{Mg} - O^{\bullet}_{O}]$, substitution of Li for Mg with the addition of a Li surface interstitial and the clustering of two Li ions with the formation of a neutral $[Li'_{Mg}V^{\bullet\bullet}_{O}Li'_{Mg}]$ oxygen vacancy. The latter two would not be expected to generate electronic holes and hence would not be expected to be catalytically active. We also present detailed analysis of hydrogen adsorption on the defective (100), (110) and (111) low index surfaces and the results will be discussed in relation to catalytic activity.

## II. COMPUTATIONAL METHODS

The periodic DFT code VASP [37, 38] was employed for all our calculations, in which a plane waves basis set describes the valence electronic states. The Perdew-Burke-Ernzerhof [39] (PBE) gradient corrected functional was used to treat the exchange and correlation. Interactions between the cores (Mg:[Be], Li:[He], H:[H] and O:[He]) and the valence electrons were described using the projector-augmented wave [40] (PAW) method. To allow correct description of the unpaired electron produced when forming an oxygen hole, all calculations were fully spin polarized with a $U$ value of 7 eV applied to the O $p$ states in all systems that contain oxygen. This value has previously been shown to be suitable for the description of polarons in this system [35].

To describe surfaces within three-dimensional periodic boundary conditions, the slab method was employed. Within this approach, the model system was constructed as a 2 x 2 supercell two-dimensional slab of finite thickness, periodically repeated in the three Cartesian dimensions. The (100), (110), and (111) MgO surfaces were cleaved from bulk MgO configurations using METADISE [41]. The periodic slabs are separated by a vacuum gap in the direction perpendicular to the surface planes, which is large enough to remove spurious slab–slab interactions. In all calculations, a vacuum thickness of 15 Å between periodic slab images was applied.

Each surface was tested for convergence of surface energy against slab thickness. This resulted in thicknesses of 12.12 Å (6 atomic layers) for the (100) surface, 11.90 Å (6 atomic layers) for the (110) surface, and 12.22 Å (13 atomic layers) for the (111) surface. A 2 x 2 x 1 $k$-point sampling mesh and a plane wave energy cutoff of 500 eV were also used for each surface to ensure suitable energy convergence. The modifications made to the atomic structure in preparing defective systems were performed identically on both sides of the slab to ensure that the slab dipole moment perpendicular to the surface was zero.

For each surface considered, a full ionic relaxation was performed after construction to find an equilibrium energy and geometry. The structures were deemed to be converged when the forces on all the ions were less than $0.01\,\text{eV}\text{Å}^{-1}$. GGA + $U$ calculations using the same calculation parameters and convergence criteria as described above were also performed on $Li_2O$, $CH_4$, $CH_3$ and $O_2$, so that consistent energies could be obtained for use in the defect formation energy calculations. The minimum distance between defect images is 8.42 Å on the (110) surface with the other defect–defect image distances being 8.42 Å for the (100), 11.91 Å for the (111) Mg terminated and 10.75 Å for the (111) O terminated.

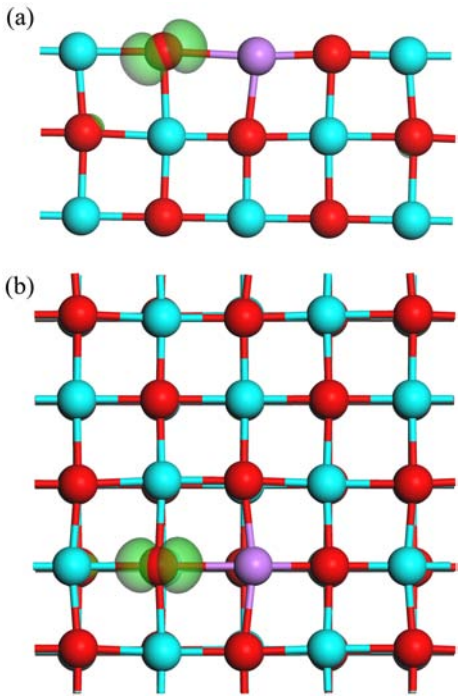


FIG. 1: Side view (upper panel) and top view (lower panel) of the relaxed GGA + $U$ geometry and partial electron density of the (100) surface of Li-doped MgO with $[Li'_{Mg} - O^{\bullet}_{O}]$ defect. The Mg atoms are coloured turquoise, Li atoms coloured purple and O atoms coloured red. The isosurface (green) shown is set at 0.05 electrons $\text{Å}^3$. This partial density was integrated between 0.8 eV and 2.3 eV.

## III. RESULTS

### A. (100) Surface

The (100) surface is a flat surface, with five coordinate oxygens and magnesiums on identical sites. The nearest neighbour Mg–O distances were 2.11 Å, which are relatively unchanged compared to the bulk, which is consistent with previous studies on the (100) surface [24]. The relaxed (100) surface energy was calculated to be $0.91\,\text{J}\,\text{m}^{-2}$.

Formation of an oxygen hole on the (100) surface consisted of replacing one Mg atom with a Li atom. An oxygen hole could form on any of the symmetry equivalent oxygen atoms in the surface layers, and hence to break the symmetry one of the neighbouring oxygens was displaced off its lattice site, increasing one Li–O bond. Figure 1 shows the GGA + $U$ relaxed geometry for the $[Li'_{Mg} - O^{\bullet}_{O}]$ defect on the (100) surface. A single increased Li–O bond length of 2.38 Å is present, together with a shortened Li–O bond length of 1.92 Å. The geometry is consistent with previous experimental [14] and theoretical [22, 23, 35] studies.

$[Li'_{Mg}V^{\bullet\bullet}_{O}Li'_{Mg}]$ was formed by replacing two magnesium surface atoms with lithiums and removing one oxygen.

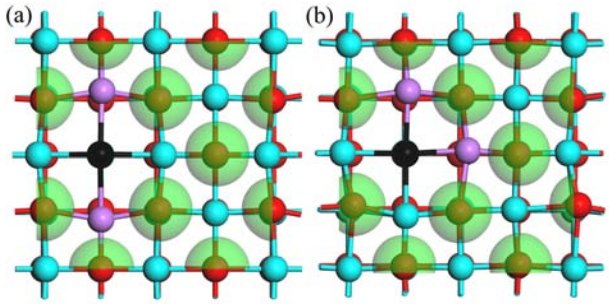


FIG. 2: The relaxed GGA + $U$ geometry and valence electron density of the (100) surface of Li-doped MgO with $[Li'_{Mg}V_O^{\bullet\bullet}Li'_{Mg}]$ defect; (a) $I_{(100)}$ and (b) $II_{(100)}$. The Mg atoms are coloured turquoise, Li atoms coloured purple and O atoms coloured red. The vacancy position is indicated schematically by a black atom. The isosurface (green) shown is set at 0.15 electrons Å$^3$.

There are two possible configurations of this defect as shown in Fig. 2. In the first configuration, the two lithiums which are either side of the vacancy form a linear chain, denoted $I_{(100)}$, and in the second the two lithium atoms are positioned forming a 90° angle around the vacancy, denoted $II_{(100)}$. In both configurations all of the sites are in the surface plane. The relaxed geometries (Fig. 2) show that the lithium atoms move away from the vacancy in both configurations making two shortened Li–O bond lengths of 1.84 Å in configuration one, and Li–O bond lengths of 1.82 Å and 1.85 Å in configuration two.

Li-doping of the (100) with an additional Li interstitial, forming a $[Li'_{Mg}Li_i^{\bullet}]$ was also considered, Fig. 3. The interstitial lithium sits above the surface plane, bridging the substituent lithium and one of the nearest neigbour oxygens. The oxygen it is coordinated to is perturbed upwards out of the plane, and the substituent lithium is perturbed downwards into bulk. This results in a $Li'_{Mg}$–$Li_i^{\bullet}$ bond length of 2.06 Å, a $Li'_{Mg}$–O bond length of 1.87 Å between the substituent lithium and its nearest neighbour oxygen in the surface and a 1.83 Å $Li'_{Mg}$–O distance between the substituent lithium and the oxygen below it in the sub surface layer. There is also a $Li_i^{\bullet}$–O bond length of 1.77 Å between the interstitial lithium and the oxygen it is coordinated to.

Analysis of the partial (ion and angular momentum decomposed) electronic density of states (PEDOS) for the $[Li'_{Mg} - O_O^{\bullet}]$, Fig. 4, shows the presence of an occupied state 5.0 eV below the valence band edge. This peak corresponds to the population of the O 2$p$ state with a single electron. A second unoccupied peak, positioned 1.0 eV above the valence band edge and in the band gap is also noted. This gap state is caused by the O 2$p$ hole trapped on the oxygen ion. EDOS plots for both the $[Li'_{Mg}V_O^{\bullet\bullet}Li'_{Mg}]$ and $[Li'_{Mg}Li_i^{\bullet}]$ defects show the absence of any unoccupied states in the band gap, which is as expected.

The partial electronic density was calculated for the region in the EDOS surrounding the gap state for the $[Li'_{Mg} - O_O^{\bullet}]$ and is shown in Fig. 1. The density is of O 2$p$ character and is localized mostly on the O ion with the elongated Li–O bond. This clearly provides a good description of the $[Li'_{Mg} - O_O^{\bullet}]$, consistent with EPR [14, 15, 17] studies and similar to UHF [22, 23] and previous GGA + $U$ [35] studies. Analysis of the valence electron density isosurfaces for the (100) oxygen vacancy configurations show that there is no accumulation of charge density in the vacancy, Fig. 2. This indicates that this defect does not result in a localized charge on the oxygen ions, and is in contrast with the $[Li'_{Mg} - O_O^{\bullet}]$ defect. The $[Li'_{Mg}Li_i^{\bullet}]$ also shows no localized charge in or neighbouring the defect, indicating a formally ionic defect.

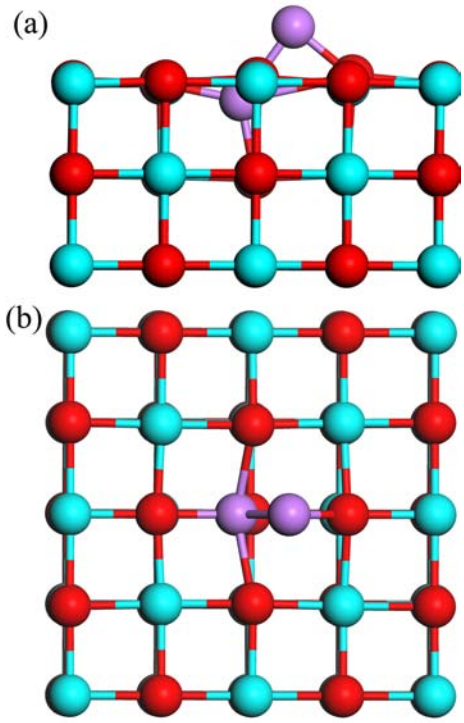


FIG. 3: The relaxed GGA + $U$ geometry of the (100) surface of Li-doped MgO with $[Li'_{Mg}Li_i^{\bullet}]$ defect. The Mg atoms are coloured turquoise, Li atoms coloured purple and O atoms coloured red. Side view (a) and top view (b).

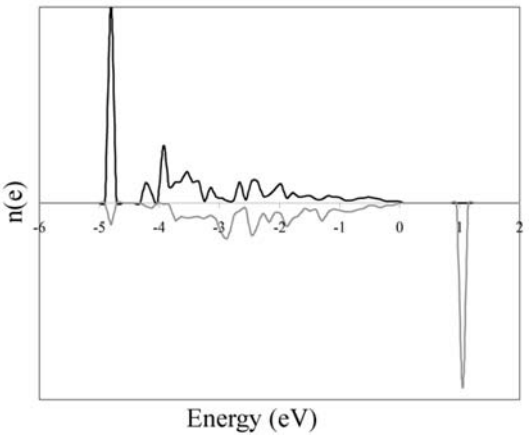


FIG. 4: O 2$p$ PEDOS for the oxygen bonded to the Li dopant with the elongated bond on the the MgO (100) with $[Li'_{Mg} - O_O^{\bullet}]$ defect ( black spin up, grey spin down). The highest occupied state is set to 0 eV.

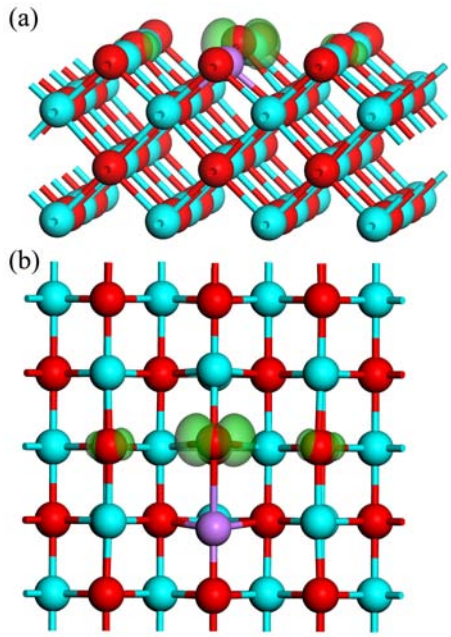


FIG. 5: Angled side view (upper panel) and top view (lower panel) of the relaxed GGA + $U$ geometry and partial electron density of the (110) surface of Li-doped MgO with [$Li'_{Mg} - O^{\bullet}_{O}$] defect. The Mg atoms are coloured turquoise, Li atoms coloured purple and O atoms coloured red. The isosurface (green) shown is set at 0.05 electrons Å$^3$. This partial density was integrated between 0.8 eV and 2.3 eV.

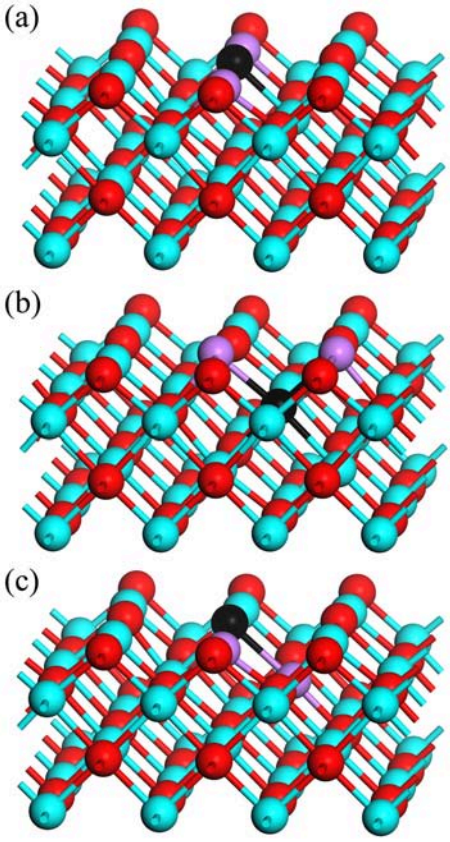


FIG. 6: The relaxed GGA + $U$ geometry of the (110) surface of Li-doped MgO with [$Li'_{Mg}V^{\bullet\bullet}_{O}Li'_{Mg}$] defect; (a) $I_{(110)}$, (b) $II_{(110)}$ and (c) $II_{(110)}$.

### B. (110) Surface

The (110) surface consists of a series of repeating upper and lower ridges (with the lower ridges being the valleys between the upper ridges) with the ridges running in the [100] direction. The surface ions are four coordinate resulting in a higher surface energy of 2.31 J m$^{-2}$. The Mg–O bond lengths along the ridges are found to be 2.12 Å, with the Mg–O bond lengths running from upper ridge to lower ridge (perpendicular to the [100] direction) being 2.11 Å. The [$Li'_{Mg} - O^{\bullet}_{O}$] defect was constructed by replacing one of the Mg atoms on the upper ridge of the (110), with distortion of one of the nearest neighbour oxygen atoms within the same upper ridge to break the symmetry. The relaxed structure is shown in Fig. 5 with one of the Li–O bond lengths increased from 2.12 Å to 2.43 Å, similar to the polaron formed on the (100).

Three different vacancy configurations were investigated on the doped (110) MgO surface. The first type, $I_{(110)}$, consists of both Li ions residing on one ridge of the surface, with the oxygen vacancy linearly between them, as shown in Fig. 6(a). The second vacancy ($II_{(110)}$) has two lithium ions sitting on adjacent ridges on the surface, with the vacancy sitting between them on the surface of the lower ridge, thus forming a 90° Li–$V$–Li angle, Fig. 6(b). In the third configuration ($III_{(110)}$), one lithium sits on an magnesium site on an upper ridge, one sits in an adjacent magnesium site on a neighbouring lower ridge, with the vacancy sitting on the upper ridge, forming a 90° Li–$V$–Li angle, Fig. 6(c). In all three cases, the lithium ions moved away from the position the oxygen had been situated in prior to vacancy formation, as did the nearest neighbour cations, but the smaller singly charged lithium substituents moved further off their sites than the magnesium ions.

On this surface, the formation of the [$Li'_{Mg}Li^{\bullet}_{i}$] defect consisted of the lithium replacing a magnesium on an upper ridge, and then the interstitial lithium sits in a position a magnesium would have held if there was a layer above it, bridging surface oxygens from adjacent ridges. This results in one elongated $Li'_{Mg}$–O bond length of 2.75 Å and one shortened $Li'_{Mg}$–O of 1.87 Å, and two $Li^{\bullet}_{i}$–O bond lengths of 1.81 Å and 1.74 Å, Fig. 7.

Analysis of the PEDOS for the [$Li'_{Mg} - O^{\bullet}_{O}$] (Fig. 8) finds a singly occupied O 2$p$ peak at 5.0 eV below the valence band edge, and a corresponding unoccupied gap state 1.9 eV above the valence band. Density of states for the [$Li'_{Mg}V^{\bullet\bullet}_{O}Li'_{Mg}$] and [$Li'_{Mg}Li^{\bullet}_{i}$] both display no defect states in the valence band-conduction band gap, similar to their corresponding compensating defects on the (100) surface.

The partial electronic density was again calculated for the region in the EDOS surrounding the gap state for the [$Li'_{Mg} - O^{\bullet}_{O}$] and is shown in Fig. 5. The excess spin is of O 2$p$ character and is localized mostly on the O ion with the elongated Li–O bond, as expected. Valence electron density isosurfaces for the (110) oxygen vacancy configurations and [$Li'_{Mg}Li^{\bullet}_{i}$] configuration show that there is no accumulation of charge density in the vacancy or around the interstitial, again indicating an essentially ionic defect.

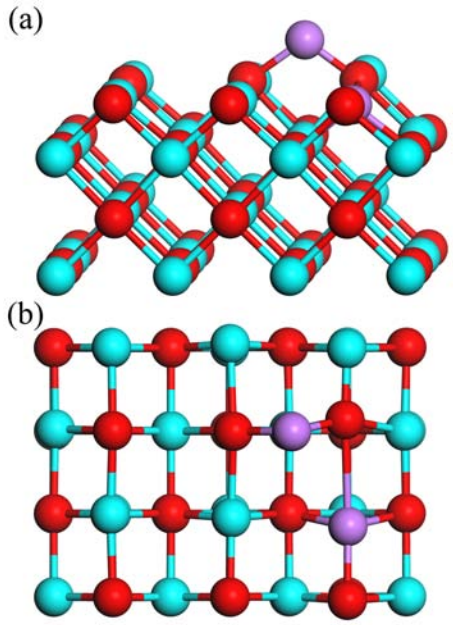


FIG. 7: The relaxed GGA + $U$ geometry of the (110) surface of Li-doped MgO with $[Li'_{Mg}Li^{\bullet}_{i}]$ defect. Side view (a) and top view (b).

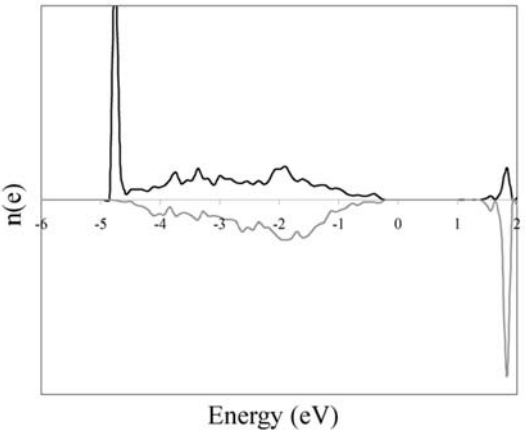


FIG. 8: O 2$p$ PEDOS for the oxygen bonded to the Li dopant with the elongated bond on the MgO (110) with $[Li'_{Mg} - O^{\bullet}_{O}]$ defect ( black spin up, grey spin down). The highest occupied state is set to 0 eV.

### C. (111) Surface

As MgO has the B1 rock salt structure, the (100) and (110) surfaces are defined by Tasker [42] as type I surfaces for which the layers are a charge neutral array of equal numbers of cations and anions. The (111) surface is type III being composed of alternating charged planes that give rise to a dipole perpendicular to the surface. As a consequence, the bulk crystal can be cleaved to form a (111) surface terminated with either cations (Mg) or anions (O); and thus we have considered both surfaces in this work. To remove the large dipole perpendicular to the surface that would otherwise be present, half the exposed atoms uppermost on one (111) surface were transferred to the opposite side of the slab in a process similar to that employed in other type III oxide surface calculations [43]. Previous DFT work has shown such a formation of (100) microfacetting to be the most stable reconstruction of the MgO (111) surface [44]. For an unmodified (111) surface, the ions that make up the uppermost surface layer (which can be oxygen or magnesium) each sit at the apex of a trigonal bipyramid, and have a coordination environment with trigonal symmetry. Transferring $[1\bar{1}1]$ rows of ions from one side of the slab to the opposite side lowers the symmetry of the surface sites, making the three counterions in the subsurface layer nonequivalent. Two remain equivalent to each other and occupy five-coordinate bridging sites, each coordinated to two surface atoms; the third lies on the other side of the surface ion in a nonbridging four-coordinate site being coordinated to a single surface ion. In what follows, these sites will be denoted $X_b$ and $X_{nb}$, where X is Mg in the case of an oxygen-terminated surface, and O in the case of a magnesium-terminated surface.

#### 1. *Mg terminated (111)*

The Mg terminated (111) has a surface energy of $3.44\,J\,m^{-2}$ and undergoes a strong distortion upon relaxation, and results in three-coordinate surface cation sites with two Mg–O interatomic distances of 1.88 Å and 1.86 Å. For the Mg terminated $[Li'_{Mg} - O^{\bullet}_{O}]$ defect, one magnesium is replaced by a lithium dopant, with the hole potentially forming on one of two inequivalent oxygens on the surface, ($O_b$ and $O_{nb}$). Two calculations were performed with each oxygen distorted from its lattice site to encourage localization. Relaxation of both starting geometries resulted in the same converged configuration, with the Li-$O_{nb}$ bond length increased from 1.86 Å to 1.89 Å, Fig. 9. Although this does not constitute as large a distortion as for the (110) and (100) surfaces, the Li-O elongation is coupled with a shortening of the other two Li-O bonds from 1.88 Å to 1.81 Å, showing the distortion and localization motif is consistent with the previous surfaces.

One oxygen vacancy configuration was calculated for the (111) Mg terminated surface, in which the two dopant lithium atoms lie in the same top-most row of ions, Fig. 10. The vacancy is in a bridging oxygen site and relaxation of the structure resulted in the Li atoms moving away from the vacancy, resulting in two Li–O bond lengths of 1.83 Å between the lithiums and the other bridging oxygen in the vacancy row, and two Li–O bond lengths of 1.70 Å between the lithiums and the nonbridging oxygens.

To construct the $[Li'_{Mg}Li^{\bullet}_{i}]$ for the (111) surface, one lithium replaces a magnesium in a surface layer, with the interstitial lithium placed in a surface interstitial site which would have been occupied by a surface magnesium atom in a non-reconstructed MgO (111). The interstitial lithium is coordinated to three oxygens (Fig. 11), with bond lengths of 1.82 Å, 1.90 Å and 1.80 Å for the $Li^{\bullet}_{i}$–O and 1.86 Å, 1.90 Å and 1.76 Å for $Li'_{Mg}$–O.

Examination of the PEDOS for the $[Li'_{Mg} - O^{\bullet}_{O}]$ reveals an unoccupied gap state 1.4 eV above the valence band, indicating the presence of a localized defect similar to those observed for the other two surfaces, Fig. 12. Density of states for the other two competing defects do

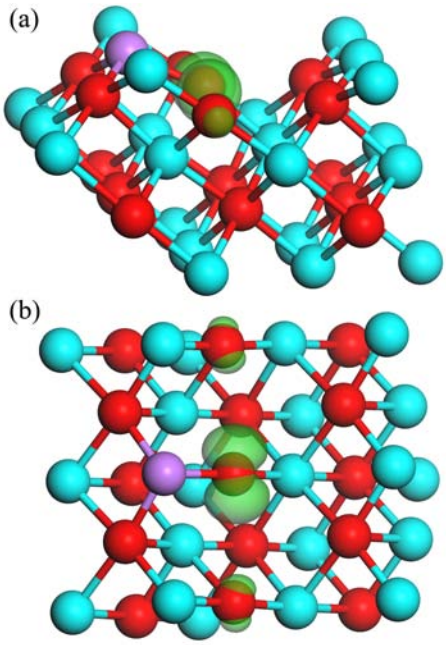


FIG. 9: Angled side view (upper panel) and top view (lower panel) of the relaxed GGA + $U$ geometry and partial electron density of the (111) Mg terminated surface of Li-doped MgO with $[Li'_{Mg} - O^{\bullet}_{O}]$ defect. The Mg atoms are coloured turquoise, Li atoms coloured purple and O atoms coloured red. The isosurface (green) shown is set at 0.05 electrons Å$^3$. This partial density was integrated between 0.8 eV and 2.3 eV.

not display any defective states in the band gap.

The partial electron density for the defect state in the $[Li'_{Mg} - O^{\bullet}_{O}]$ case shows strong localization on the O of the elongated Li–O bond, further evidence of a localized polaron. Valence electron density charge plots for the $[Li'_{Mg}V^{\bullet\bullet}_{O}Li'_{Mg}]$ and $[Li'_{Mg}Li^{\bullet}_{i}]$ defects again show no accumulation of charge around the defects, showing close to formal ions for these configurations.

### *2. O terminated 111*

The oxygen terminated (111), with a surface energy of 3.58 J m$^{-2}$, possesses two distinct types of cation site at which Li can be introduced, the bridging ($Mg_b$) and non-bridging ($Mg_nb$) sites. The surface non-bridging site is four-coordinate with two Mg–O distances of 2.20 Å, one of 1.99 Å and one of 1.86 Å. The bridging cation site is five-coordinate, with two Mg–O distances of 2.28 Å, two of 1.88 Å and one of 2.19 Å. Calculations were performed on both configurations, and in both cases, elongation of one Li–O bond was found. For the bridging dopant site, a Li–O bond length of 2.19 Å was (up from 1.88 Å in the pure surface) noted. Similarly for the non-bridging dopant site, the Li–O bond length increases from 1.86 Å in the pure surface to 1.89 Å. The relaxed structure for the non-bridging $[Li'_{Mg} - O^{\bullet}_{O}]$ defect, which is the most stable doping site, is shown in Fig. 13. Similar to the (111) Mg terminated surface, the elongation of the Li–O bond is not as large as on the (110) and (100) surfaces, but is coupled with a shortening of the two Li-O subsurface bond lengths to 1.98 Å from 2.20 Å.

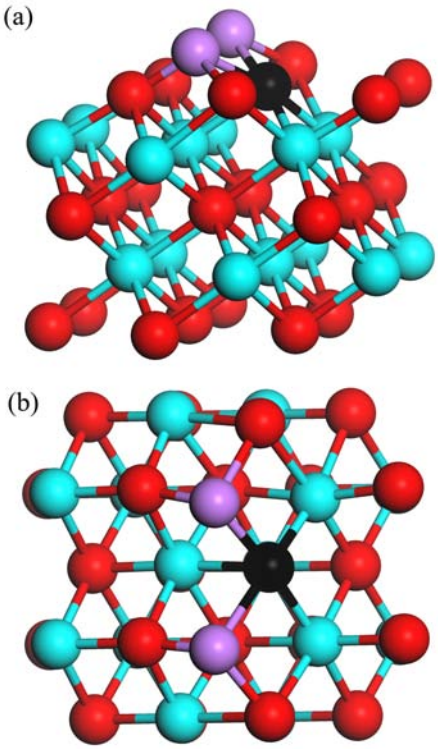


FIG. 10: The relaxed GGA + $U$ geometry of the (111) Mg terminated surface of Li-doped MgO with $[Li'_{Mg}V^{\bullet\bullet}_{O}Li'_{Mg}]$ defect; (a) side angled view and (b) plan view. The Mg atoms are coloured turquoise, Li atoms coloured purple and O atoms coloured red. The vacancy position is indicated schematically by a black sphere.

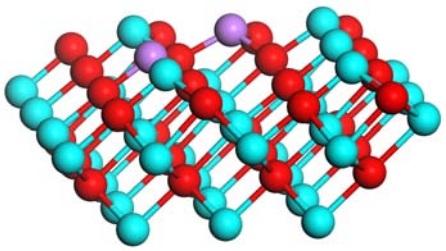

FIG. 11: The relaxed GGA + $U$ geometry of the (111) Mg terminated surface of Li-doped MgO with $[Li'_{Mg}Li^{\bullet}_{i}]$ defect. The Mg atoms are coloured turquoise, Li atoms coloured purple and O atoms coloured red.

Two different vacancy configurations were also considered on the (111) oxygen terminated surface. The vacancy site in both cases is a surface terminating oxygen site. Each surface terminating oxygen site has three neighbouring cation sites, two bridging and one non bridging, two of which are substituted by Li in forming the vacancy. This results in two possible structures, ($I_{(111o)}$) where one Li atom occupies the non-bridging site and one of the (equivalent) bridging sites forming a $Li_b - V - Li_{nb}$ motif, or ($II_{(111o)}$) where both of the bridging sites are substituted forming $Li_b - V - Li_b$. In both cases, the two Li ions are distorted away from their initial positions and drawn towards the bulk, with $I_{(111o)}$ (Fig. 14(a)) having Li–O interatomic distances of 1.91 Å and 2.02 Å and $II_{(111o)}$ having Li–O bond lengths of 1.83 Å, Fig. 14(b).

Formation of the $[Li'_{Mg}Li^{\bullet}_{i}]$ defect on the oxygen termi-

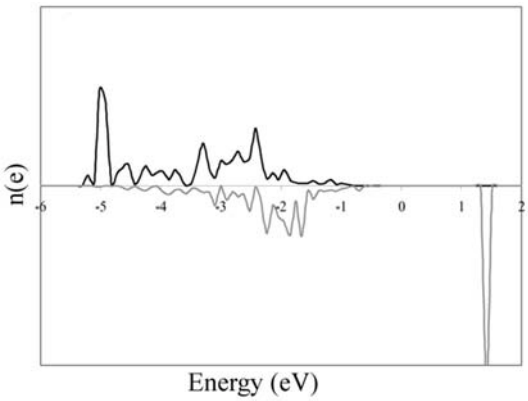


FIG. 12: O 2*p* PEDOS for the oxygen bonded to the Li dopant with the elongated bond on the MgO (111) Mg terminated surface with $[\mathrm{Li}'_{\mathrm{Mg}} - \mathrm{O}^{\bullet}_{\mathrm{O}}]$ defect ( black spin up, grey spin down). The highest occupied state is set to 0 eV.

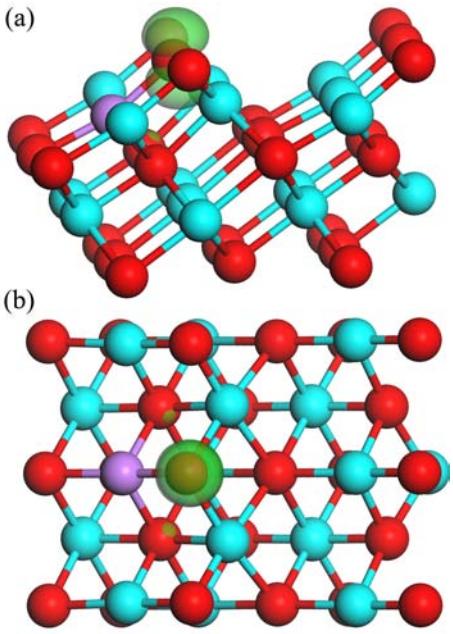


FIG. 13: Angled side view (upper panel) and top view (lower panel) of the relaxed GGA + *U* geometry and partial electron density of the (111) O terminated surface of Li-doped MgO with $[\mathrm{Li}'_{\mathrm{Mg}} - \mathrm{O}^{\bullet}_{\mathrm{O}}]$ defect. The Mg atoms are coloured turquoise, Li atoms coloured purple and O atoms coloured red. The isosurface (green) shown is set at 0.05 electrons $\mathring{A}^3$. This partial density was integrated between 0.8 eV and 2.3 eV.

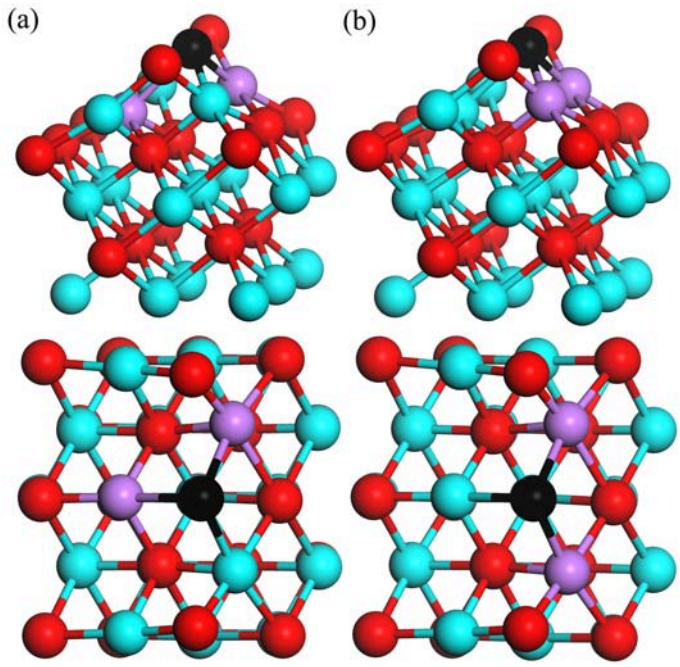


FIG. 14: The relaxed GGA + *U* geometry of the (111) O terminated surface of Li-doped MgO with $[\mathrm{Li}'_{\mathrm{Mg}} V^{\bullet\bullet}_{\mathrm{O}} \mathrm{Li}'_{\mathrm{Mg}}]$ defect; (a) $\mathrm{I}_{(111\mathrm{o})}$ and (b) $\mathrm{II}_{(111\mathrm{o})}$. The Mg atoms are coloured turquoise, Li atoms coloured purple and O atoms coloured red. The vacancy position is indicated schematically by a black atom.

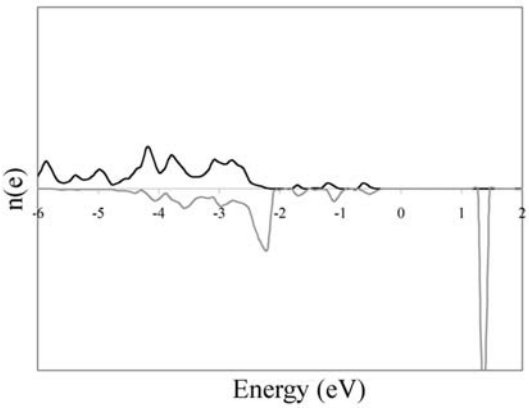


FIG. 15: O 2*p* PEDOS for the oxygen bonded to the Li dopant with the elongated bond on the the MgO (111) O terminated surface with $[\mathrm{Li}'_{\mathrm{Mg}} - \mathrm{O}^{\bullet}_{\mathrm{O}}]$ defect ( black spin up, grey spin down). The highest occupied state is set to 0 eV.

nated surface would be electrostatically unfavourable, as the interstitial sites (which would be occupied by oxygen atoms in a non-reconstructed surface) have three neighbouring Mg cations. Thus no attempt was made to model such a high energy configuration.

Examination of the PEDOS for both hole configurations shows that the normal lower energy peak seen in the other three terminations is coupled with the main O 2*p* valence band. The unoccupied state still appears in the band gap 1.4 eV above the valence band similar to the (111) Mg terminated oxygen hole which is higher than the unoccupied states on the (100) and lower than the (110), Fig. 15. The EDOS for the vacancy configurations show no gap states, as was expected. Partial electron density plots for the non-bridging $[\mathrm{Li}'_{\mathrm{Mg}} - \mathrm{O}^{\bullet}_{\mathrm{O}}]$ show that the localization is on the O ion with the extended Li–O interatomic distance, Fig. 13. Similar results were obtained for the bridging oxygen hole.

### D. Energetics

The energy of formation of the $[\mathrm{Li}'_{\mathrm{Mg}} - \mathrm{O}^{\bullet}_{\mathrm{O}}]$ defect for each surface can be calculated by the following equation:

$$\mathrm{MgO}_{\mathrm{slab}} + \mathrm{Li_2O} + \frac{1}{2}\mathrm{O_2} \rightarrow \mathrm{MgO}\left(2\left[\mathrm{Li}-\mathrm{O}\right]\right)_{\mathrm{slab}} + 2\mathrm{MgO} \quad (1)$$

The formation energies of the vacancy configurations are calculated according to:

$$\mathrm{MgO_{slab}}+2\mathrm{Li_2O}+\frac{1}{2}\mathrm{O_2} \rightarrow \mathrm{MgO}\left(2\left[2\mathrm{Li}+\mathrm{O_{vac}}\right]\right)_{\mathrm{slab}}+4\mathrm{MgO} \quad (2)$$

The $[\mathrm{Li}'_{\mathrm{Mg}}\mathrm{Li}^{\bullet}_{\mathrm{i}}]$ formation energies are calculated using the equation:

$$\mathrm{MgO_{slab}}+2\mathrm{Li_2O} \rightarrow \mathrm{MgO}\left(2\left[2\mathrm{Li}\right]\right)_{\mathrm{slab}}+2\mathrm{MgO} \quad (3)$$

The defect energetics for the three surfaces are shown in Table I. The formation of all the defects on the (100) surface costs energy, with the $[\mathrm{Li}'_{\mathrm{Mg}}-\mathrm{O}^{\bullet}_{\mathrm{O}}]$ and the $[\mathrm{Li}'_{\mathrm{Mg}}\mathrm{Li}^{\bullet}_{\mathrm{i}}]$ defects the most likely to form, with both having formation energies of $+0.51\,\mathrm{eV\,Li^{-1}}$.

On the (110) surface, the formation of the oxygen hole is most energetically favourable, with a gain in energy of $1.58\,\mathrm{eV\,Li^{-1}}$. The most energetically favourable vacancy is the $\mathrm{I}_{(110)}$, with a formation of $-0.99\,\mathrm{eV\,Li^{-1}}$. The formation of the $[\mathrm{Li}'_{\mathrm{Mg}}\mathrm{Li}^{\bullet}_{\mathrm{i}}]$ also results in an energy gain, but is not as favourable as $[\mathrm{Li}'_{\mathrm{Mg}}-\mathrm{O}^{\bullet}_{\mathrm{O}}]$ formation.

On both (111) terminations, the formation of the oxygen hole is clearly more favourable, with the (111) Mg terminated polaron having a formation energy of $-2.04\,\mathrm{eV\,Li^{-1}}$, and the hole formed with the lithium on a non-bridging site on the (111) O terminated surface having a formation energy of $-2.06\,\mathrm{eV\,Li^{-1}}$. These large favourable energies probably reflect the inherent instability of the (111) surfaces.

### E. Hydrogen absorption

In Lunsford's [8] mechanism for the oxidative coupling of methane over Li-doped MgO, the first step in the cycle is hydrogen abstraction by $[\mathrm{Li}'_{\mathrm{Mg}}-\mathrm{O}^{\bullet}_{\mathrm{O}}]$ defects, with formation of a surface OH group. This is also considered to be the rate limiting step in the cycle and is thus of major importance [7]. Thus we consider the interaction of H with the $[\mathrm{Li}'_{\mathrm{Mg}}-\mathrm{O}^{\bullet}_{\mathrm{O}}]$ on all the surface terminations. The structures of these Li-OH motifs are shown in Fig. 16. The distance from the Li to the hydroxyl oxygen on the (100) surface is 2.46 Å and the H-O bond length is 0.96 Å. The hydrogen is tilted toward the Li, which has been noted in previous studies [24, 35]. The formation of the hydroxyl group on the (110) surfaces again results in an elongated Li–O bond length of 2.58 Å and a H–O bond length of 0.96 Å. On the (111) Mg terminated surface the H tilts away from the Li, with a Li–O bond length of 1.90 Å and an O–H length of 0.97 Å. For the (111) O terminated surface the hydrogen binds normal to the surface, with O–H and Li–O bond lengths of 0.96 Å and 1.95 Å respectively.

Analysis of the EDOS for these systems shows no gap state present in the bandgap, with a doubly occupied state lying $\sim 6.8\,\mathrm{eV}$ below the valence band edge. Thus the hydrogen has filled the previously unoccupied gap state. The EDOS for the Li–O–H motif on the (100) is shown in Fig. 17.

The reaction considered for the abstraction of methane over Li-doped MgO is:

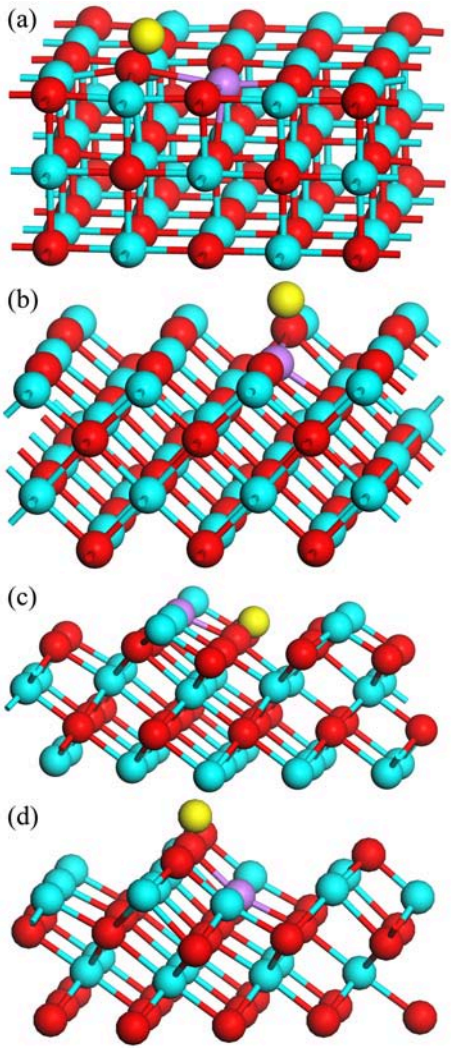


FIG. 16: The relaxed GGA + $U$ geometry of the H adsorbed on (a) (100), (b) (110), (c) (111) Mg terminated and (d) (111) O terminated. Mg atoms are coloured turquoise, Li atoms coloured purple, O atoms coloured red and H atoms coloured yellow.

$$2\mathrm{CH_4}+\mathrm{MgO}\left(2\left[\mathrm{Li}-\mathrm{O}\right]\right)_{\mathrm{slab}} \rightarrow \mathrm{MgO}\left(2\left[\mathrm{Li}-\mathrm{O}-\mathrm{H}\right]\right)_{\mathrm{slab}}+2\mathrm{CH_3} \quad (4)$$

with one hydrogen adsorbed onto each side of the slab. The energies of hydrogen abstraction are shown in Table II. The energy to abstract hydrogen onto the (100) surface is calculated to be 1.09 eV, which is consistent with the previous GGA + $U$ calculated energy of 1.21 eV [35]. The calculated abstraction energies for the (110), (111) Mg terminated and (111) O terminated are 1.12 eV, 1.21 eV and 0.81 eV respectively. This does indicate that the oxygen terminated (111) surface of MgO significantly lowers the reaction energy compared to the other terminations.

## IV. DISCUSSION/CONCLUSION

In this paper we have considered the GGA $+U$ description of the competing defect mechanisms on Li-doped

TABLE I: Formation energies for the three competing defects on the low index surfaces of MgO. The notations (nb) and (b) denote non-bridging and bridging sites and roman numerals denote different lithium positions.

| | $[Li'_{Mg} - O^{\bullet}_{O}]$ | $[Li'_{Mg}V^{\bullet\bullet}_{O}Li'_{Mg}]$ | $[Li'_{Mg}Li^{\bullet}_{i}]$ |
|---|---|---|---|
| (100) | +0.51 eV | +0.65 eV | +0.51 eV |
| (110) | −1.58 eV | (I)−0.99 eV, (II)+0.52 eV, (III)−0.27 eV | −0.59 eV |
| (111)Mg | −2.04 eV | −0.70 eV | 0.59 eV |
| (111)O | (nb)−2.06 eV, (b)−1.08 eV | (I)−0.70 eV, (II)0.59 eV | |

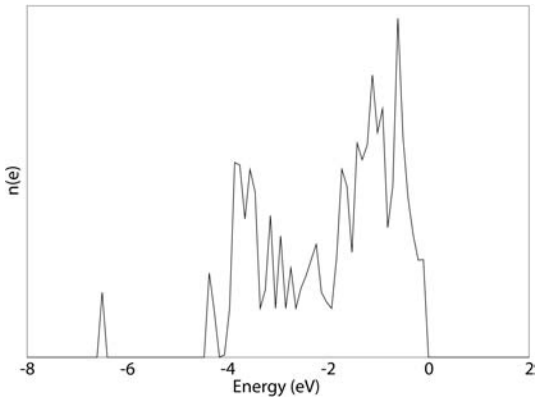


FIG. 17: Total EDOS for the Li-doped MgO (100) surface with an adsorbed hydrogen. The highest occupied state is set to 0 eV.

TABLE II: The hydrogen abstraction energy by the $[Li'_{Mg} - O^{\bullet}_{O}]$ on the (100), (110) and (111) surfaces of MgO.

| Surface | Energy |
|---|---|
| (100) | 1.09eV |
| (110) | 1.12eV |
| (111)Mg | 1.21eV |
| (111)O | 0.81eV |

MgO low index surfaces. The effect of Li-doping with electronic hole compensation on the geometry is qualitatively the same for all the surface terminations, showing an elongation of the Li–O bond and displaying unoccupied gap states in the band gap, with localization of the electronic hole on a single oxygen site (the oxygen ion involved in the Li–O elongated bond). This demonstrates the formation of a potentially catalytically active centre, on each of the low index surfaces.

Formation of the $[Li'_{Mg}V^{\bullet\bullet}_{O}Li'_{Mg}]$ and $[Li'_{Mg}Li^{\bullet}_{i}]$ defects on the four terminations were also considered. The formation of the $[Li'_{Mg}V^{\bullet\bullet}_{O}Li'_{Mg}]$ defect produces similar results on each surface, with the two Li ions perturbed away from the vacancy, with no electrons present in the vacancy site, and no gap state in the EDOS. The absence of charge in the vacancy site points to the defect being catalytically inactive, on all surface terminations.

The $[Li'_{Mg}Li^{\bullet}_{i}]$ defect also displayed results that were qualitatively the same for each of the three surfaces, and similar to the $[Li'_{Mg}V^{\bullet\bullet}_{O}Li'_{Mg}]$ defects showed no gap states in the EDOS and as such is another catalytically inactive defect center.

Analysis of the energetics of the competing defect mechanisms shows that all three defect mechanisms cost energy to form on the (100), with the $[Li'_{Mg} - O^{\bullet}_{O}]$ and $[Li'_{Mg}Li^{\bullet}_{i}]$ defects being equally favoured, indicating that the (100) is not a good candidate as an OCM catalyst. The formation of the $[Li'_{Mg} - O^{\bullet}_{O}]$ on the other terminations is energetically favourable, and this defect is clearly the most energetically favourable on these surfaces.

Finally the adsorption of hydrogen to the $[Li'_{Mg} - O^{\bullet}_{O}]$ defect has been investigated, with in all cases the hydrogen filling the unoccupied gap state present in the PEDOS of the $[Li'_{Mg} - O^{\bullet}_{O}]$ defect. The energetics of H abstraction indicate that catalysis over the O terminated (111) could significantly lower the reaction energy.

The (100) has by far the lowest surface energy and is therefore the most likely to form. However the competition between polaron and $[Li'_{Mg}Li^{\bullet}_{i}]$ formation is relatively even, meaning that only about 50% of the defects on the (100) surface will be the catalytically active $[Li'_{Mg} - O^{\bullet}_{O}]$ defect. This is in contrast with the (110) and both terminations of the (111) where polaron formation is heavily favoured. Therefore exposing the (110) and (111) surfaces could lead to a significant increase in the catalytic activity of Li-doped MgO, since it is likely that lithium will segregate to these surfaces and will preferentially lead to oxygen hole formation. Thus upon lithium doping of MgO the Li will segregate to the (110) and (111) surfaces generating catalytically active sites and hence the (110) and (111) surfaces will demonstrate high catalytic activity.

### Acknowledgments

We acknowledge support for this work from Science Foundation Ireland (Grant Numbers 04/BR/C0216 and 05/RFP/CHE0035) and the HEA for the PTRLI programs: IITAC (Cycle III) and e-INIS (CYCLE IV). All calculations were performed on the IITAC supercomputer as maintained by the Trinity Centre for High Performance Computing (TCHPC).

[1] J. H. Lunsford, Catal. Today **6**, 235 (1990).
[2] T. Ito and J. H. Lunsford, Nature **314**, 721 (1985).
[3] J. A. Roos, S. J. Korf, R. H. J. Veehof, J. G. Van Ommen, and J. R. H. Ross, Appl. Catal. **52**, 147 (1989).
[4] R. H. Nibbelke, J. Scheerová, M. H. J. M. de Groon, and G. B. Marin, J. Catal. **156**, 106 (1995).
[5] P. M. Couwenberg, Q. Chen, and G. B. Marin, Ind. Eng. Chem. Res. **35**, 3999 (1996).

[6] H. Aritani, H. Yamada, T. Nishio, T. Shiono, S. Imamura, M. Kudo, S. Hasegawa, T. Tanaka, and S. Yoshida, J. Phys. Chem. B **104**, 10133 (2000).
[7] L. Leveles, K. Seshan, J. A. Lercher, and L. Lefferts, J. Catal. **218**, 296 (2003).
[8] T. Ito, J. -X. Wang, C. -H. Lin, and J. H. Lunsford, J. Am. Chem. Soc. **107**, 5062 (1985).
[9] D. J. Driscoll and J. H. Lunsford, J. Phys. Chem. **89**, 4415 (1985).
[10] K. D. Campbell, E. Morales, and J. H. Lunsford, J. Am. Chem. Soc. **109**, 7900 (1987).
[11] K. D. Campbell and J. H. Lunsford, J. Phys. Chem. **92**, 5792 (1988).
[12] J. H. Lunsford, *Methane Conversion by Oxidative Processes* (Van Nostrand Reinhold, 1992).
[13] M. -C. Wu, C. M. Truong, and D. W. Goodman, Phys. Rev. B. **46**, 12694 (1992).
[14] M. M. Abraham, W. P. Unruh, and Y. Chen, Phys. Rev. B.**10**, 3540 (1974).
[15] M. M. Abraham, Y. Chen, L. A. Boatner, R. W. Reynolds, Phys. Rev. Lett. **37**, 849 (1976).
[16] Y. Chen, H. T. Tohver, J. Narayan, M. M. Abraham, Phys. Rev. B. **16**, 5535 (1977).
[17] J. B. Lacy, M. M Abraham, J. L. Boldú O, Y. Chen, J. Narayan, and H. T. Tohver, Phys. Rev. B **18**, 4136 (1978).
[18] G. J. Hutchings, M. S. Scurrell, and J. R. Woodhouse, J. Chem. Soc., Chem. Comm. **12**, 765 (1989).
[19] D. J. Lunsford, W. Martir, J. X. Wang, and J. H. Lunsford, J. Am. Chem. Soc. **107**, 58 (1985).
[20] C. R. A. Catlow, *Quantum Mechanical Cluster Calculations in Solid State Studies* (World Scientific, Singapore 1992).
[21] M. Lintuluoto and Y. Nakamura, J. nol. Struct. Theochem. **674**, 207 (2004).
[22] A. Lachinot, C. Larrieu, R. Orlando, and R. Dovesi, J. Phys. Chem. Sol. **59**, 7 (1998).
[23] R. Dovesi, R. Orlando, C. Roetti, C. Pisani, and R. V. Saunders, Phys. Stat. Sol. B. **217**, 63 (2000).
[24] L. K. Dash and M. J. Gillan, Surf. Sci. **549**, 217 (2004).
[25] J. Laesgaard and K. Stokbor, Phys. Rev. B **65**, 075208 (2002).
[26] A. Chainani, M. Mathew, and D. D. Sarma, Phys. Rev. B **46**, 9961 (1992).
[27] N. Nolan and G. W. Watson. J. Chem. Phys. **125**, 144701 (2006).
[28] A. Chainani, M. Mathew, and D. D. Sarma, Phys. Rev. B **48**, 14818 (1993).
[29] D. O. Scanlon, A. Walsh, B. J. Morgan, and G. W. Watson, J. Phys. Chem. C **112**, 9903 (2008).
[30] B. J. Morgan and G. W. Watson, Surf. Sci. **601**, 5034 (2007).
[31] M. Nolan, S. Grigoleit, D. C. Sayle, S. C. Parker, and G. W. Watson, Surf. Sci. **576**, 217 (2005).
[32] L. Ackermann, J. D. Gale, C. R. A. Catlow, and A. Andersson, J. Phys. Chem. B **42**, 263 (1982).
[33] S. L. Dudarev, G. A. Botton, S. Y. Savrasov, C. J. Humphreys, and A. P. Sutton, Phys. Rev. B. **57**, 1505 (1998).
[34] I. V. Anisimov, J. Zaanen, and O. K. Andersen, Phys. Rev. B **44**, 943 (1991).
[35] M. Nolan and G. W. Watson, Surf. Sci. **586**, 25 (2005).
[36] D. O. Scanlon, A. Walsh, B. J. Morgan, M. Nolan, J. Fearon, and G. W. Watson, J. Phys. Chem. C **111**, 7971 (2007).
[37] G. Kresse and J. Furthmuller, Comp. Mat. Sci. **6**, 15 (1996).
[38] G. Kresse and J. Hafner, Phys. Rev. B **49**, 14251 (1994).
[39] J. P. Perdew, K. Burke, and M. Ernzerhof, Phys. Rev. Lett. **77**, 3865 (1996).
[40] P. E. Blöchl, Phys. Rev. B **50**, 17953 (1994).
[41] G. W. Watson, E. T. Kelsey, N. H. de Leeuw, D. J. Harris, and S. C. Parker **92**, 433 (1996).
[42] P. W. Tasker, J. Phys. C: Solid State Phys. **12**, 4977 (1979).
[43] P. M. Oliver, S. C. Parker, and W. C. Macrodt, Mod. Simul. Mater. Sci. Eng. **1**, 755 (1993).
[44] A. Wander, I. Bush, and N. M. Harrison, Phys. Rev. B. **68**, 233405 (2003).